Search for neutrino lines from dark matter annihilation and decay with IceCube

R. Abbasi,[17] M. Ackermann,[64] J. Adams,[18] S. K. Agarwalla,[41,*] J. A. Aguilar,[12] M. Ahlers,[22] J. M. Alameddine,[23] N. M. Amin,[45] K. Andeen,[43] G. Anton,[26] C. Argüelles,[14] Y. Ashida,[41] S. Athanasiadou,[64] S. N. Axani,[45] X. Bai,[51] A. Balagopal,[41] M. Baricevic,[41] S. W. Barwick,[30] V. Basu,[41] S. Baur,[12] R. Bay,[8] J. J. Beatty,[20,21] K.-H. Becker,[63] J. Becker Tjus,[11,†] J. Beise,[62] C. Bellenghi,[27] S. BenZvi,[53] D. Berley,[19] E. Bernardini,[49] D. Z. Besson,[36] G. Binder,[8,9] D. Bindig,[63] E. Blaufuss,[19] S. Blot,[64] F. Bontempo,[31] J. Y. Book,[14] C. Boscolo Meneguolo,[49] S. Böser,[42] O. Botner,[62] J. Böttcher,[1] E. Bourbeau,[22] J. Braun,[41] B. Brinson,[6] J. Brostean-Kaiser,[64] R. T. Burley,[2] R. S. Busse,[44] D. Butterfield,[41] M. A. Campana,[50] K. Carloni,[14] E. G. Carnie-Bronca,[2] S. Chattopadhyay,[41,*] N. Chau,[12] C. Chen,[6] Z. Chen,[56] D. Chirkin,[41] S. Choi,[57] B. A. Clark,[19] L. Classen,[44] A. Coleman,[62] G. H. Collin,[15] A. Connolly,[20,21] J. M. Conrad,[15] P. Coppin,[13] P. Correa,[13] S. Countryman,[47] D. F. Cowen,[60,61] P. Dave,[6] C. De Clercq,[13] J. J. DeLaunay,[59] D. Delgado López,[14] H. Dembinski,[45] K. Deoskar,[55] A. Desai,[41] P. Desiati,[41] K. D. de Vries,[13] G. de Wasseige,[38] T. DeYoung,[24] A. Diaz,[15] J. C. Díaz-Vélez,[41] M. Dittmer,[44] A. Domi,[26] H. Dujmovic,[41] M. A. DuVernois,[41] T. Ehrhardt,[42] C. El Aisati,[12] P. Eller,[27] R. Engel,[31,32] H. Erpenbeck,[41] J. Evans,[19] P. A. Evenson,[45] K. L. Fan,[19] K. Fang,[41] A. R. Fazely,[7] A. Fedynitch,[58] N. Feigl,[10] S. Fiedlschuster,[26] C. Finley,[55] L. Fischer,[64] D. Fox,[60] A. Franckowiak,[11] E. Friedman,[19] A. Fritz,[42] P. Fürst,[1] T. K. Gaisser,[45] J. Gallagher,[40] E. Ganster,[1] A. Garcia,[14] L. Gerhardt,[9] A. Ghadimi,[59] C. Glaser,[62] T. Glauch,[27] T. Glüsenkamp,[26,62] N. Goehlke,[32] J. G. Gonzalez,[45] S. Goswami,[59] D. Grant,[24] S. J. Gray,[19] S. Griffin,[41] S. Griswold,[53] C. Günther,[1] M. Gustafsson,[12] P. Gutjahr,[23] C. Haack,[27] A. Hallgren,[62] R. Halliday,[24] L. Halve,[1] F. Halzen,[41] T. Hambye,[12] H. Hamdaoui,[56] M. Ha Minh,[27] K. Hanson,[41] J. Hardin,[15] A. A. Harnisch,[24] P. Hatch,[33] A. Haungs,[31] K. Helbing,[63] J. Hellrung,[11] F. Henningsen,[27] L. Heuermann,[1] N. Heyer,[62] S. Hickford,[63] A. Hidvegi,[55] C. Hill,[16] G. C. Hill,[2] K. D. Hoffman,[19] K. Hoshina,[41,‡] W. Hou,[31] T. Huber,[31] K. Hultqvist,[55] M. Hünnefeld,[23] R. Hussain,[41] K. Hymon,[23] S. In,[57] A. Ishihara,[16] M. Jacquart,[41] M. Jansson,[55] G. S. Japaridze,[5] K. Jayakumar,[41,*] M. Jeong,[57] M. Jin,[14] B. J. P. Jones,[4] D. Kang,[31] W. Kang,[57] X. Kang,[50] A. Kappes,[44] D. Kappesser,[42] L. Kardum,[23] T. Karg,[64] M. Karl,[27] A. Karle,[41] U. Katz,[26] M. Kauer,[41] J. L. Kelley,[41] A. Khatee Zathul,[41] A. Kheirandish,[34,35] J. Kiryluk,[56] S. R. Klein,[8,9] A. Kochocki,[24] R. Koirala,[45] H. Kolanoski,[10] T. Kontrimas,[27] L. Köpke,[42] C. Kopper,[24] D. J. Koskinen,[22] P. Koundal,[31] M. Kovacevich,[50] M. Kowalski,[10,64] T. Kozynets,[22] K. Kruiswijk,[38] E. Krupczak,[24] A. Kumar,[64] E. Kun,[11] N. Kurahashi,[50] N. Lad,[64] C. Lagunas Gualda,[64] M. Lamoureux,[38] M. J. Larson,[19] F. Lauber,[63] J. P. Lazar,[14,41] J. W. Lee,[57] K. Leonard DeHolton,[60,61] A. Leszczyńska,[45] M. Lincetto,[11] Q. R. Liu,[41] M. Liubarska,[25] E. Lohfink,[42] C. Love,[50] C. J. Lozano Mariscal,[44] L. Lu,[41] F. Lucarelli,[28] A. Ludwig,[37] W. Luszczak,[20,21] Y. Lyu,[8,9] J. Madsen,[41] K. B. M. Mahn,[24] Y. Makino,[41] S. Mancina,[41,49] W. Marie Sainte,[41] I. C. Mariş,[12] S. Marka,[47] Z. Marka,[47] M. Marsee,[59] I. Martinez-Soler,[14] R. Maruyama,[46] F. Mayhew,[24] T. McElroy,[25] F. McNally,[39] J. V. Mead,[22] K. Meagher,[41] S. Mechbal,[64] A. Medina,[21] M. Meier,[16] S. Meighen-Berger,[27] Y. Merckx,[13] L. Merten,[11] J. Micallef,[24] T. Montaruli,[28] R. W. Moore,[25] Y. Morii,[16] R. Morse,[41] M. Moulai,[41] T. Mukherjee,[31] R. Naab,[64] R. Nagai,[16] M. Nakos,[41] U. Naumann,[63] J. Necker,[64] M. Neumann,[44] H. Niederhausen,[24] M. U. Nisa,[24] A. Noell,[1] S. C. Nowicki,[24] A. Obertacke Pollmann,[16] V. O'Dell,[41] M. Oehler,[31] B. Oeyen,[29] A. Olivas,[19] R. Orsoe,[27] J. Osborn,[41] E. O'Sullivan,[62] H. Pandya,[45] N. Park,[33] G. K. Parker,[4] E. N. Paudel,[45] L. Paul,[43] C. Pérez de los Heros,[62] J. Peterson,[41] S. Philippen,[1] S. Pieper,[63] A. Pizzuto,[41] M. Plum,[51] A. Pontén,[62] Y. Popovych,[42] M. Prado Rodriguez,[41] B. Pries,[24] R. Procter-Murphy,[19] G. T. Przybylski,[9] J. Rack-Helleis,[42] K. Rawlins,[3] Z. Rechav,[41] A. Rehman,[45] P. Reichherzer,[11] G. Renzi,[12] E. Resconi,[27] S. Reusch,[64] W. Rhode,[23] M. Richman,[50] B. Riedel,[41] E. J. Roberts,[2] S. Robertson,[8,9] S. Rodan,[57] G. Roellinghoff,[57] M. Rongen,[42] C. Rott,[54,57] T. Ruhe,[23] L. Ruohan,[27] D. Ryckbosch,[29] S. Athanasiadou,[64] I. Safa,[14,41] J. Saffer,[32] D. Salazar-Gallegos,[24] P. Sampathkumar,[31] S. E. Sanchez Herrera,[24] A. Sandrock,[23] M. Santander,[59] S. Sarkar,[25] S. Sarkar,[48] J. Savelberg,[1] P. Savina,[41] M. Schaufel,[1] H. Schieler,[31] S. Schindler,[26] B. Schlüter,[44] F. Schlüter,[12] T. Schmidt,[19] J. Schneider,[26] F. G. Schröder,[31,45] L. Schumacher,[27] G. Schwefer,[1] S. Sclafani,[50] D. Seckel,[45] S. Seunarine,[52] R. Shah,[50] A. Sharma,[62] S. Shefali,[32] N. Shimizu,[16] M. Silva,[41] B. Skrzypek,[14] B. Smithers,[4] R. Snihur,[41] J. Soedingrekso,[23] A. Søgaard,[22] D. Soldin,[32] G. Sommani,[11] C. Spannfellner,[27] G. M. Spiczak,[52] C. Spiering,[64] M. Stamatikos,[21] T. Stanev,[45] T. Stezelberger,[9] T. Stürwald,[63] T. Stuttard,[22] G. W. Sullivan,[19] I. Taboada,[6] S. Ter-Antonyan,[7] W. G. Thompson,[14] J. Thwaites,[41] S. Tilav,[45] K. Tollefson,[24] C. Tönnis,[57] S. Toscano,[12] D. Tosi,[41] A. Trettin,[64] C. F. Tung,[6] R. Turcotte,[31] J. P. Twagirayezu,[24] B. Ty,[41] M. A. Unland Elorrieta,[44] A. K. Upadhyay,[41,*] K. Upshaw,[7] N. Valtonen-Mattila,[62] J. Vandenbroucke,[41] N. van Eijndhoven,[13] D. Vannerom,[15] J. van Santen,[64] J. Vara,[44] J. Veitch-Michaelis,[41] M. Venugopal,[31] S. Verpoest,[29] D. Veske,[47] C. Walck,[55] T. B. Watson,[4] C. Weaver,[24] P. Weigel,[15] A. Weindl,[31] J. Weldert,[60,61] C. Wendt,[41] J. Werthebach,[23] M. Weyrauch,[31] N. Whitehorn,[24,37] C. H. Wiebusch,[1]

N. Willey,[24] D. R. Williams,[59] M. Wolf,[27] G. Wrede,[26] X. W. Xu,[7] J. P. Yanez,[25] E. Yildizci,[41] S. Yoshida,[16] F. Yu,[14] S. Yu,[24] T. Yuan,[41] Z. Zhang,[56] and P. Zhelnin[14]

(IceCube Collaboration)

[1]*III. Physikalisches Institut, RWTH Aachen University, D-52056 Aachen, Germany*
[2]*Department of Physics, University of Adelaide, Adelaide, Adelaide 5005, Australia*
[3]*Department of Physics and Astronomy, University of Alaska Anchorage, 3211 Providence Drive, Anchorage, Alaska 99508, USA*
[4]*Department of Physics, University of Texas at Arlington, 502 Yates Street, Science Hall Room 108, Box 19059, Arlington, Texas 76019, USA*
[5]*CTSPS, Clark-Atlanta University, Atlanta, Georgia 30314, USA*
[6]*School of Physics and Center for Relativistic Astrophysics, Georgia Institute of Technology, Atlanta, Georgia 30332, USA*
[7]*Department of Physics, Southern University, Baton Rouge, Louisiana 70813, USA*
[8]*Department of Physics, University of California, Berkeley, California 94720, USA*
[9]*Lawrence Berkeley National Laboratory, Berkeley, California 94720, USA*
[10]*Institut für Physik, Humboldt-Universität zu Berlin, D-12489 Berlin, Germany*
[11]*Fakultät für Physik and Astronomie, Ruhr-Universität Bochum, D-44780 Bochum, Germany*
[12]*Université Libre de Bruxelles, Science Faculty CP230, B-1050 Brussels, Belgium*
[13]*Vrije Universiteit Brussel (VUB), Dienst ELEM, B-1050 Brussels, Belgium*
[14]*Department of Physics and Laboratory for Particle Physics and Cosmology, Harvard University, Cambridge, Massachusetts 02138, USA*
[15]*Department of Physics, Massachusetts Institute of Technology, Cambridge, Massachusetts 02139, USA*
[16]*Department of Physics and The International Center for Hadron Astrophysics, Chiba University, Chiba 263-8522, Japan*
[17]*Department of Physics, Loyola University Chicago, Chicago, Illinois 60660, USA*
[18]*Department of Physics and Astronomy, University of Canterbury, Private Bag 4800, Christchurch, New Zealand*
[19]*Department of Physics, University of Maryland, College Park, Maryland 20742, USA*
[20]*Department of Astronomy, Ohio State University, Columbus, Ohio 43210, USA*
[21]*Department of Physics and Center for Cosmology and Astro-Particle Physics, Ohio State University, Columbus, Ohio 43210, USA*
[22]*Niels Bohr Institute, University of Copenhagen, DK-2100 Copenhagen, Denmark*
[23]*Department of Physics, TU Dortmund University, D-44221 Dortmund, Germany*
[24]*Department of Physics and Astronomy, Michigan State University, East Lansing, Michigan 48824, USA*
[25]*Department of Physics, University of Alberta, Edmonton, Alberta T6G 2E1, Canada*
[26]*Erlangen Centre for Astroparticle Physics, Friedrich-Alexander-Universität Erlangen-Nürnberg, D-91058 Erlangen, Germany*
[27]*Physik-department, Technische Universität München, D-85748 Garching, Germany*
[28]*Département de physique nucléaire et corpusculaire, Université de Genève, CH-1211 Genève, Switzerland*
[29]*Department of Physics and Astronomy, University of Gent, B-9000 Gent, Belgium*
[30]*Department of Physics and Astronomy, University of California, Irvine, California 92697, USA*
[31]*Karlsruhe Institute of Technology, Institute for Astroparticle Physics, D-76021 Karlsruhe, Germany*
[32]*Karlsruhe Institute of Technology, Institute of Experimental Particle Physics, D-76021 Karlsruhe, Germany*
[33]*Department of Physics, Engineering Physics, and Astronomy, Queen's University, Kingston, Ontario K7L 3N6, Canada*
[34]*Department of Physics and Astronomy, University of Nevada, Las Vegas, Nevada, 89154, USA*
[35]*Nevada Center for Astrophysics, University of Nevada, Las Vegas, Nevada 89154, USA*
[36]*Department of Physics and Astronomy, University of Kansas, Lawrence, Kansas 66045, USA*
[37]*Department of Physics and Astronomy, UCLA, Los Angeles, California 90095, USA*
[38]*Centre for Cosmology, Particle Physics and Phenomenology—CP3, Université catholique de Louvain, Louvain-la-Neuve, Belgium*
[39]*Department of Physics, Mercer University, Macon, Georgia 31207-0001, USA*
[40]*Department of Astronomy, University of Wisconsin–Madison, Madison, Wisconsin 53706, USA*
[41]*Department of Physics and Wisconsin IceCube Particle Astrophysics Center, University of Wisconsin–Madison, Madison, Wisconsin 53706, USA*
[42]*Institute of Physics, University of Mainz, Staudinger Weg 7, D-55099 Mainz, Germany*
[43]*Department of Physics, Marquette University, Milwaukee, Wisconsin, 53201, USA*

[44]Institut für Kernphysik, Westfälische Wilhelms-Universität Münster, D-48149 Münster, Germany
[45]Bartol Research Institute and Department of Physics and Astronomy, University of Delaware, Newark, Delaware 19716, USA
[46]Department of Physics, Yale University, New Haven, Connecticut 06520, USA
[47]Columbia Astrophysics and Nevis Laboratories, Columbia University, New York, New York 10027, USA
[48]Department of Physics, University of Oxford, Parks Road, Oxford OX1 3PU, United Kingdom
[49]Dipartimento di Fisica e Astronomia Galileo Galilei, Università Degli Studi di Padova, 35122 Padova PD, Italy
[50]Department of Physics, Drexel University, 3141 Chestnut Street, Philadelphia, Pennsylvania 19104, USA
[51]Physics Department, South Dakota School of Mines and Technology, Rapid City, South Dakota 57701, USA
[52]Department of Physics, University of Wisconsin, River Falls, Wisconsin 54022, USA
[53]Department of Physics and Astronomy, University of Rochester, Rochester, New York 14627, USA
[54]Department of Physics and Astronomy, University of Utah, Salt Lake City, Utah 84112, USA
[55]Oskar Klein Centre and Department of Physics, Stockholm University, SE-10691 Stockholm, Sweden
[56]Department of Physics and Astronomy, Stony Brook University, Stony Brook, New York 11794-3800, USA
[57]Department of Physics, Sungkyunkwan University, Suwon 16419, South Korea
[58]Institute of Physics, Academia Sinica, Taipei, 11529, Taiwan
[59]Department of Physics and Astronomy, University of Alabama, Tuscaloosa, Alabama 35487, USA
[60]Department of Astronomy and Astrophysics, Pennsylvania State University, University Park, Pennsylvania 16802, USA
[61]Department of Physics, Pennsylvania State University, University Park, Pennsylvania 16802, USA
[62]Department of Physics and Astronomy, Uppsala University, Box 516, S-75120 Uppsala, Sweden
[63]Department of Physics, University of Wuppertal, D-42119 Wuppertal, Germany
[64]Deutsches Elektronen-Synchrotron DESY, Platanenallee 6, 15738 Zeuthen, Germany

(Received 27 March 2023; accepted 7 July 2023; published 8 November 2023)

Dark matter particles in the Galactic Center and halo can annihilate or decay into a pair of neutrinos producing a monochromatic flux of neutrinos. The spectral feature of this signal is unique and it is not expected from any astrophysical production mechanism. Its observation would constitute a dark matter smoking gun signal. We performed the first dedicated search with a neutrino telescope for such signal, by looking at both the angular and energy information of the neutrino events. To this end, a total of five years of IceCube's DeepCore data has been used to test dark matter masses ranging from 10 GeV to 40 TeV. No significant neutrino excess was found and upper limits on the annihilation cross section, as well as lower limits on the dark matter lifetime, were set. The limits reached are of the order of 10^{-24} cm^3/s for an annihilation and up to 10^{27} s for decaying dark matter. Using the same data sample we also derive limits for dark matter annihilation or decay into a pair of Standard Model charged particles.

DOI: 10.1103/PhysRevD.108.102004

I. INTRODUCTION

The existence of dark matter in the Milky Way and beyond can be probed indirectly through the observation of various kinds of particle fluxes produced by its annihilation or decay [1–3]. Looking at this possibility with neutrinos is of special interest because, as opposed to charged cosmic rays, neutrinos can propagate over very long distances without being deflected by magnetic fields. Moreover, neutrinos are much less absorbed than photons, in particular by the interstellar medium at very high energies or in dense environments. Because of these two properties neutrinos point back to their origin of emission, even if this origin is far away or very dense, such as the center of the Sun or the center of Earth [4–6].

In this article, we search for monochromatic fluxes of neutrinos that could have been emitted by annihilation or decay of dark matter in the Milky Way. Monochromatic fluxes of neutrinos are produced when the parent particle is nonrelativistic (as expected in the inner part of the Galaxy) and those processes proceed into two-body final states where at least one of the two particles is a neutrino. In the following we will assume that the second particle is also a neutrino, i.e., we consider the $\chi\chi \to \nu\bar{\nu}$ and $\chi \to \nu\bar{\nu}$ processes. The results we will get under this assumption can also be used for the case where the final state would consist of a single neutrino and another unknown particle, modulo a factor 2 for the neutrino flux and taking into

[*]Also at Institute of Physics, Sachivalaya Marg, Sainik School Post, Bhubaneswar 751005, India.
[†]Also at Department of Space, Earth and Environment, Chalmers University of Technology, 412 96 Gothenburg, Sweden.
[‡]Also at Earthquake Research Institute, University of Tokyo, Bunkyo, Tokyo 113-0032, Japan.

account the shift of the neutrino line toward lower energies if the mass of this unknown particle is not negligible. The neutrino line scenario is different from the usual setting where dark matter first creates a flux of Standard Model primary particles, leading to a continuum flux of secondary neutrinos from the subsequent decay (and hadronization) of these primary particles [7].

The search of a monochromatic flux of neutrinos is interesting for at least four reasons. First, when the signal has a narrow spectral feature it is easier to identify an excess against a broad continuous background stemming from atmospheric muons and neutrinos. This is of particular relevance for IceCube's so-called cascade events that comprise neutrinos with a better energy resolution compared to tracks [8] (see Sec. II for details). Second, there is no high-energy astrophysical source that could mimic a monochromatic signal. Thus, the observation of a line feature would constitute a dark matter "smoking gun" signal. Third, for the neutrino channel, neutrino telescopes can directly probe the primary neutrinos and thus have a clear advantage over gamma-ray telescopes (which in this case can only see secondary gamma rays radiated by the neutrinos), despite the smaller neutrino interaction cross section. Finally, unlike γ-line production which generally proceeds at loop level (due to the electromagnetic neutrality of the dark matter particle, see e.g. [9]), neutrino-line production can proceed at tree level. Systematic lists of simple tree level annihilation models can be found in [10,11], and there exist numerous models where dark matter undergoes two-body decays into neutrinos, see e.g. [12–27], including models where the decay is induced by the neutrino mass seesaw interactions, see e.g. [25–27].

IceCube has already performed searches of dark matter annihilating into a pair of neutrinos [28–31]; however, these searches only used the angular information. In Ref. [32], based on two years of public data the authors showed that, given IceCube's energy resolution in cascade events, the search for a neutrino line with neutrino telescopes is clearly feasible and that the use of the energy information, crucial to distinguish a line from a continuum, allows for a clear improvement of the sensitivity.[1] Here we use both the angular and energy distributions of the events, from five years of data consisting mostly of cascade events, with an optimized data selection for a monochromatic flux search from 10 GeV to 40 TeV. An energy resolution for these cascade events of ∼30% for energies above 100 GeV is achieved. Additionally, we also used the same data sample to get new constraints on an annihilation or decay into other charged particles. Again, the energy information of the events makes it possible to improve on the expected sensitivity. In total in this study we considered the annihilation and decay into the three neutrino channels, $\nu_\mu\bar{\nu}_\mu$, $\nu_e\bar{\nu}_e$, $\nu_\tau\bar{\nu}_\tau$, and into a pair of $\tau^-\tau^+$, W^+W^-, $\mu^+\mu^-$, and $b\bar{b}$ quarks.

[1]See also [33,34] for an early estimate on the sensitivity to neutrino lines by assuming an energy resolution typical to muon track events.

This article is structured as follows: Section II gives an overview of the IceCube Neutrino Observatory and the data selection used in this analysis. The signal expectation from dark matter annihilation and decay from the Galactic Center is described in Sec. III. In Sec. IV we describe the methodology and statistical tools used. Section V reviews the source of systematic uncertainties. Results are given in Sec. VI for the neutrino channel and in Sec. VII for other channels, and conclusions are given in Sec. VIII.

II. ICECUBE AND DATA SELECTION

The IceCube Neutrino Observatory [35] is a neutrino telescope located at the South Pole and buried between 1.5 and 2.5 km in the Antarctic ice sheet. It consists of a three-dimensional array of 5,160 photo-multipliers (PMTs) that detect the Cherenkov light induced by charge particles created in the neutrino interactions with the surrounding matter. The PMTs are housed in the digital optical modules (DOMs), which also contain the electronics for the digitization of the signal [36]. DOMs are separated 17 m vertically and 125 m horizontally to optimize the detection of TeV neutrinos. A denser subarray of the IceCube detector with a reduced DOM spacing, called DeepCore [37], is located at the bottom center of the IceCube array and it is sensitive to neutrinos with energies $\gtrsim$10 GeV. Depending on the neutrino interaction, different signatures can be observed within the instrumented volume of IceCube. Charge-current interactions of ν_μ will leave a tracklike signature, while neutral-current interactions of all flavors and charge-current interactions of ν_e will induce a hadronic or electromagnetic shower leaving a spherical light pattern in the detector, which we call cascades. The same is true for charge-current interactions of ν_τ, since at energies below 1 PeV the τ decay length is shorter than the average distance of IceCube's DOMs rendering the τ track undetectable.

The event selection used in this analysis was developed for DeepCore and was optimized to identify and select cascade events [7]. Filtered data use DeepCore's fiducial volume while the neighboring strings of IceCube are used as a veto from atmospheric muons. The final selection uses boosted decision trees (BDTs) [38] trained with scrambled data as background and different reference signals from Monte Carlo (MC) simulations. Two different signal benchmarks were used: a neutrino spectra generated from a 100 GeV dark matter mass annihilating into $b\bar{b}$ and a 300 GeV mass dark matter particle annihilating into W^+W^-. Although in this analysis we focused on direct annihilation and decay into neutrinos, the choice of the two spectra used in BDTs was made to represent a soft and hard neutrino spectrum, respectively. This improves the sensitivity over a wide range of masses as well as different spectra. The scores produced by the two BDTs were used to define two different event selections, one optimized for best sensitivity of the analysis for dark matter masses from

10 GeV to 1 TeV and the other for masses from 1 toward 40 TeV.

The energy resolution, defined as the standard deviation of $E_{\rm rec}/E_{\rm true}$ distribution, improves from 60% at 10 GeV to 30% beyond 100 GeV. Both datasets also have a similar median angular resolution, ranging from ∼50° for soft annihilation channels like $b\bar{b}$ to ∼20° for the W^+W^- annihilation channel at a dark matter mass of 300 GeV, which is sufficient to exploit the directional information for large extended regions of emission such as the Galactic dark matter halo.

III. SIGNAL EXPECTATION

Since neutrinos can travel unhindered through the Galaxy, the neutrino energy spectrum remains almost identical to the spectrum at the production site. The differential neutrino flux from dark matter annihilation in an observational volume at angular distance toward the Galactic Center Ψ can be written as

$$\frac{\mathrm{d}\phi_\nu}{\mathrm{d}E_\nu}(E_\nu,\Psi)=\frac{1}{4\pi}\frac{\langle\sigma v\rangle}{2m_\chi^2}\frac{\mathrm{d}N_\nu}{\mathrm{d}E_\nu}\int_{\Delta\Omega}\int_{\rm LOS}\rho_\chi^2(r(\ell,\Psi))\mathrm{d}\ell\mathrm{d}\Omega, \quad (1)$$

where $\langle\sigma v\rangle$ is the thermally averaged dark matter self-annihilation cross section, and m_χ is the dark matter mass. The factor 2 in the denominator assumes that dark matter is a Majorana particle and therefore its own antiparticle [39]. Likewise, the differential neutrino flux from a decaying dark matter can be expressed in terms of the decaying lifetime τ_χ as

$$\frac{\mathrm{d}\phi_\nu}{\mathrm{d}E_\nu}(E_\nu,\Psi)=\frac{1}{4\pi}\frac{1}{\tau_\chi m_\chi}\frac{\mathrm{d}N_\nu}{\mathrm{d}E_\nu}\int_{\Delta\Omega}\int_{\rm LOS}\rho_\chi(r(\ell,\Psi))\mathrm{d}\ell\mathrm{d}\Omega. \quad (2)$$

In both cases the last two integrals encompass all the astrophysical information given by the dark matter density distribution in the Milky Way, $\rho_\chi(r(\ell,\Psi))$, and they are usually referred as the J-factor and D-factor, respectively (see Fig. 1),

$$J\text{-factor}\equiv\int_{\Delta\Omega}\mathcal{J}\,\mathrm{d}\Omega=\int_{\Delta\Omega}\int_{\rm LOS}\rho_\chi^2(r(\ell,\Psi))\mathrm{d}\ell\mathrm{d}\Omega,$$
$$D\text{-factor}\equiv\int_{\Delta\Omega}\mathcal{D}\,\mathrm{d}\Omega=\int_{\Delta\Omega}\int_{\rm LOS}\rho_\chi(r(\ell,\Psi))\mathrm{d}\ell\mathrm{d}\Omega. \quad (3)$$

The argument $r(\ell,\Psi)$ is the Galactocentric distance expressed as a function of the angle with respect to the Galactic Center Ψ. The differential $\mathcal{J}$-factor and $\mathcal{D}$-factor are integrated over the distance along the line of sight (LOS) ℓ. The total J-factor and D-factors include the integration over the field of view $\Delta\Omega$. The dark matter density distribution is inferred from first principles, numerical simulations, and astronomical observation and it is subject to large uncertainties [42]. As it is custom in indirect searches of dark matter, the signal predictions and results are evaluated for two different assumptions of the density profile. In this article, we used the Navarro-Frenk-White (NFW) [40] and Burkert [41] profiles. Both of them assume a spherical dark matter distribution but with a different radial profile. In this work we assumed the parameters and parametrization given in [43]. As can be seen in Fig. 1, the annihilation signal expectation is more impacted by the choice of the density profile than the decay signal, due to its dependency on ρ_χ^2 in the J-factor compared to the ρ_χ dependency in the D-factor.

The term $\mathrm{d}N_\nu/\mathrm{d}E_\nu$ describes the number of neutrinos per energy unit, at a given energy E_ν produced per annihilation or decay at the source. For the $\chi\chi\to\nu_\alpha\bar{\nu}_\alpha$ and $\chi\to\nu_\alpha\bar{\nu}_\alpha$

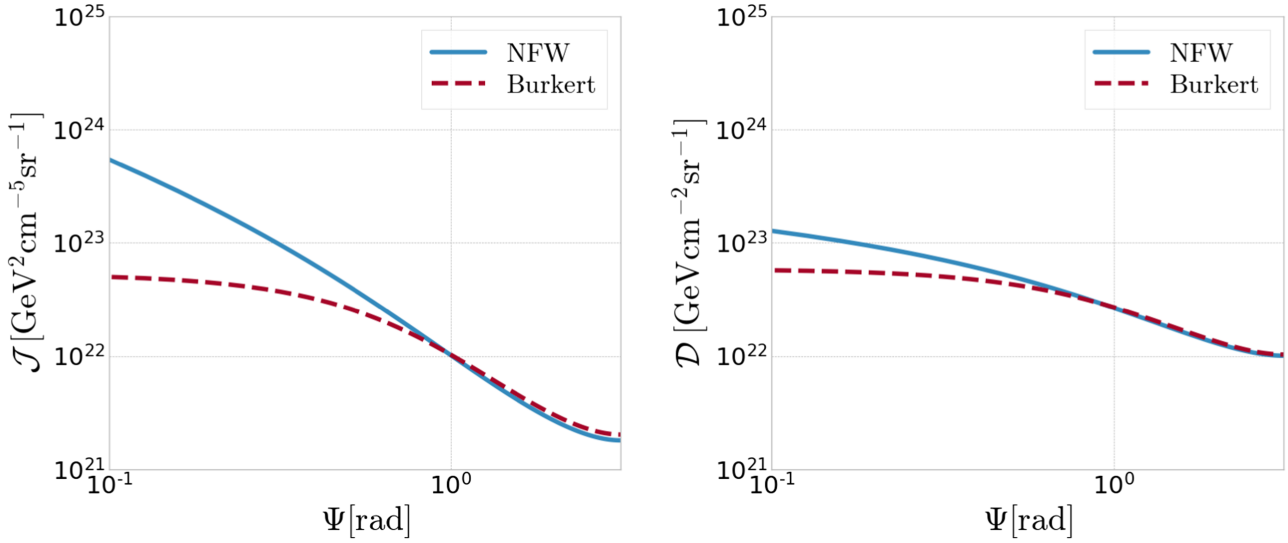

FIG. 1. Differential $\mathcal{J}$-factor (left) and $\mathcal{D}$-factor (right) per stereoradian, as a function of the angular orientation toward the Galactic Center for two assumptions of the dark matter density profile $\rho_\chi(r)$, the NFW [40] in solid blue and the Burkert [41] profile in dotted red.

channels (with $\alpha = e, \mu, \tau$), the spectra can be described by a δ-function centered at $E_\nu = m_\chi$ and $E_\nu = m_\chi/2$, respectively. Note that electroweak corrections increase the amount of low-energy neutrinos altering the monochromatic spectra in nontrivial ways. In this study, we used neutrino spectra calculated in the "poor particle physicist cookbook" (PPPC4) [44], which includes electroweak corrections at leading order as described in more detail in [45] (for a more recent treatment of electroweak corrections see [46]). For the neutrino-line channels the continuum of lower-energy neutrinos induced by the electroweak corrections is negligible for our analysis. For an annihilation or decay into a pair of charged particles, the secondary neutrino spectra from parton showers and hadronization are also estimated using the tables provided in PPPC4 [44].

For all channels studied a branching ratio of 100% is assumed at the source, including those into each monochromatic neutrino flavor line. However, long baseline vacuum neutrino oscillations will produce a similar amount of electron, muon, and tau neutrinos [32,47]. Simplistically, we take all our neutrino signals to have a democratic flavor composition when arriving at the detector.[2]

For the decay mode, as only one dark matter particle is needed to produce a decaying signal, an additional extra-Galactic and potential Galactic substructure components can have a sizable contribution. However, for angular distances of less than 30° with respect to the Galactic Center, these extra components are typically negligible for both decaying and annihilating dark matter and are therefore not considered in this analysis [32,48].

IV. ANALYSIS METHOD

In this analysis we used a Poisson binned likelihood method with two observables: the reconstructed energy of the event $E_{\rm rec}$ and the angular distance with respect to the Galactic Center $\Psi_{\rm rec}$. The likelihood expression can be written as

$$\mathcal{L}(\mu) = \prod_{i=0}^{N_{\rm bins}} \text{Poisson}(n_i | N_{\rm obs}^{\rm total} \cdot f_i(\mu)), \tag{4}$$

where maximization is performed against the signal fraction, $\mu = n_s/N_{\rm obs}^{\rm total} \in [0, 1]$, where n_s is the number of signal events in the sample and $N_{\rm obs}^{\rm total}$ is the total number of events observed. The latter is taken from data and therefore is not a free parameter of the model. For each bin in the energy-angular distance space, the expected number of events is given by $N_{\rm obs}^{\rm total} \cdot f_i(\mu)$, where $f_i(\mu)$ is the fraction of events falling in the ith bin, given by

$$f_i(\mu) = (1 - \mu) \cdot \mathcal{B}_i + \mu \cdot \mathcal{S}_i, \tag{5}$$

where $\mathcal{S}_i$ and $\mathcal{B}_i$ are the signal and background probability density functions (PDFs), respectively. A common neutrino telescope procedure is to build the background model from experimental data by scrambling the right ascension coordinate. This technique consists of assigning a uniformly random distributed right ascension to the events in order to create a background pseudosample. This is possible since neutrino telescopes have a nearly constant duty cycle and as Earth rotates the atmospheric neutrino and muon backgrounds become uniform in right ascension. Scrambling is a powerful technique but it dilutes the signal and renders the analysis insensitive to any signal contribution that is uniform in right ascension. In order to correct for a possible signal *contamination* in the background estimate, we make use of a signal subtraction likelihood [7]. In this case, the estimated background-only PDF can be written as

$$\mathcal{B}_i(\mu) = \frac{1}{1 - \mu} [\mathcal{D}_i^{\rm scrambled} - \mu \mathcal{S}_i^{\rm scrambled}], \tag{6}$$

where $\mathcal{S}^{\rm scrambled}$ is the PDF of a right ascension scrambled signal computed from simulation and $\mathcal{D}^{\rm scrambled}$ is the scrambled data. The final expression for the signal fraction can be written as

$$f_i(\mu) = \mathcal{D}_i^{\rm scrambled} + \mu \cdot (\mathcal{S}_i - \mathcal{S}_i^{\rm scrambled}). \tag{7}$$

Figure 2 shows the background PDF built from an average of 100 right ascension scrambled pseudosamples for both the low-energy (left) and the high-energy selections (right). Data distributions have a small number of events at the tails of the energy distributions. In order to avoid empty bins in the background PDF, which might be specially problematic for monochromatic signal expectations, we used a binning based on quantiles resulting in each bin containing roughly the same amount of events. This limits the statistical error per bin in the estimation of the PDF from scrambled data. The implementation of the quantile binning was done using the software PHYST.[3]

The binning used for the background PDF is then applied to the signal distributions. The signals' PDFs are built by reweighting neutrino MC simulations according to the expression given by Eqs. (1) and (2). These MC datasets include simulation of all three neutrino flavors. In order to reduce the impact of weighted MC errors, the simulation was oversampled by replicating events by a factor 200 (100 for the Burkert profile) at different arrival times while reducing by the same factor their weight. This technique produces a smooth signal distribution while preserving the energy and angular response of the detector. The signal

[2]Since the monochromatic neutrino-line spectra are basically identical for all flavors, this is in practice the same as assuming that these signals have democratic flavor composition at the source.

[3]https://github.com/janpipek/physt/.

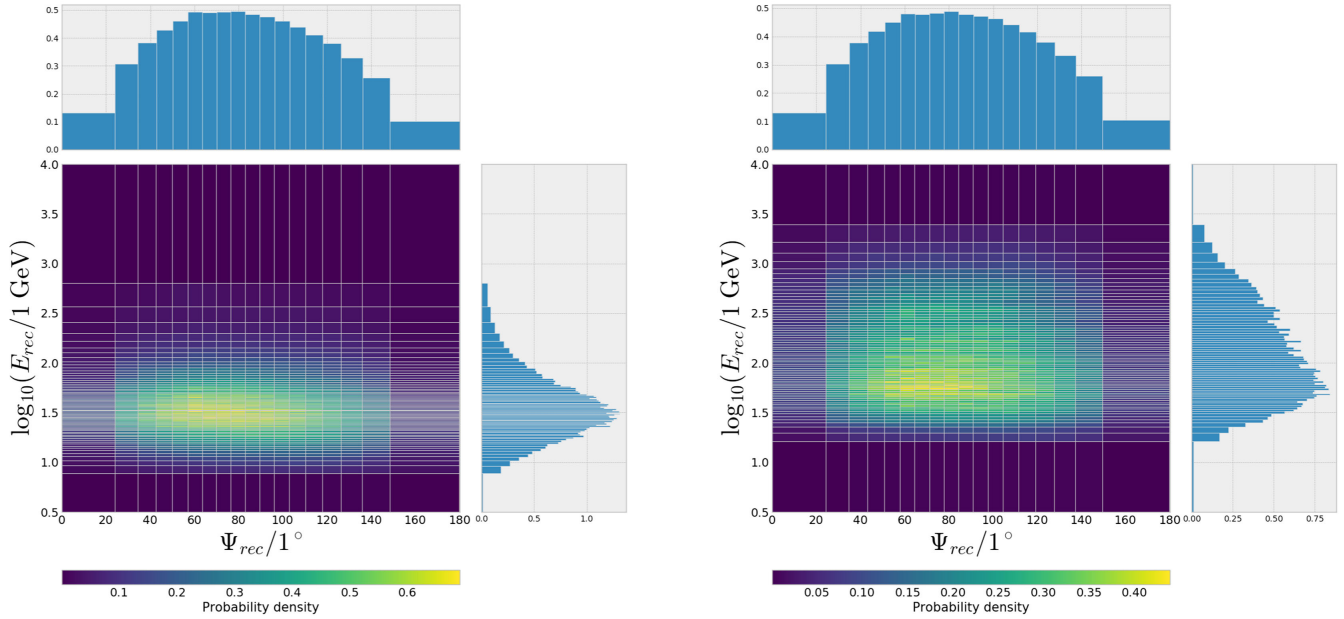

FIG. 2. Background probability density functions for the low-energy (left) and high-energy selections (right) as functions of the reconstructed energy and the angular distance toward the Galactic Center. The nonuniform binning was used in order to ensure that no empty bins are present in the distributions.

depends on the dark matter mass, the halo profile, and the annihilation or decay channel.

The top row in Fig. 3 (left) shows the signal PDF for the benchmark annihilation channel to $\nu_e\bar{\nu}_e$ and a dark matter mass of 1 TeV assuming the NFW profile. As can be seen in the projected distribution of reconstructed energy, the spectra features a sharp peak corresponding to the monochromatic signal. The right panel shows the same distribution but scrambled in right ascension. As expected from the scrambled method we consider, the projected distribution in reconstructed energy remains identical. The scrambled signal distribution is used in the minimization in order to correct the background PDF as shown in Eq. (6). For completeness, we also show in the bottom row the PDF for the case of neutrinos from a decaying dark matter into a soft channel $b\bar{b}$, assuming the Burkert profile.

In this analysis, we tested about 19 different values for the dark matter mass ranging from 10 GeV to 40 TeV. The final number of masses was selected by verifying that an injected signal in between two consecutive masses will be recovered, while at the same time limiting the computational hurdle of evaluating a large number of masses. As mentioned in Sec. I, in addition to the three neutrino channels, we also evaluate the neutrino signal coming from the W^+W^-, $\tau^+\tau^-$, $b\bar{b}$, and $\mu^+\mu^-$ channels for both annihilation and decaying dark matter and the two halo profiles. For each combination of mass, channel, and halo profile, the analysis finds the $\hat{\mu}$ that maximizes the likelihood. This best estimate can then be translated to a thermally averaged annihilation cross section $\langle\sigma v\rangle$ or a decaying dark matter lifetime τ_χ. The significance of the result, or compatibility with the null hypothesis $\mathcal{H}_0(\mu = 0)$, is calculated using the discovery test statistics q_0, defined as

$$q_0 = \begin{cases} -2\log\frac{\mathcal{L}(\hat{\mu})}{\mathcal{L}(\mu=0)} & \hat{\mu} \geq 0, \\ 0 & \hat{\mu} < 0, \end{cases} \tag{8}$$

where we assume that the physical parameter must be positive, $\mu \geq 0$, so that null hypothesis can only be rejected when the data prefer a positive signal contribution.

V. SYSTEMATIC UNCERTAINTIES

Since the background PDF is built essentially from data, there are no systematic uncertainties affecting the shape of the background model. The influence on the scrambled signal PDF from systematic uncertainties only affects slightly the background estimate for very large signal fractions. Still, signals' PDFs can have notable fluctuations, because they are based on a limited number of MC events and the technique of oversampling those. By comparing the results from the practically identical signals $\nu_e\bar{\nu}_e$, $\nu_\mu\bar{\nu}_\mu$, and $\nu_\tau\bar{\nu}_\tau$—recall that these neutrino lines' energy spectra have negligibly different electroweak corrections and democratic flavor compositions at the detector—we see from Tables I–III in the Appendix that limits are essentially unaffected, differing by few tens of percents and reaching a factor of 3 for the lowest mass. These variations can be attributed to the signals' PDFs, which are derived from independent oversampling realizations of weighted events from MC simulations.

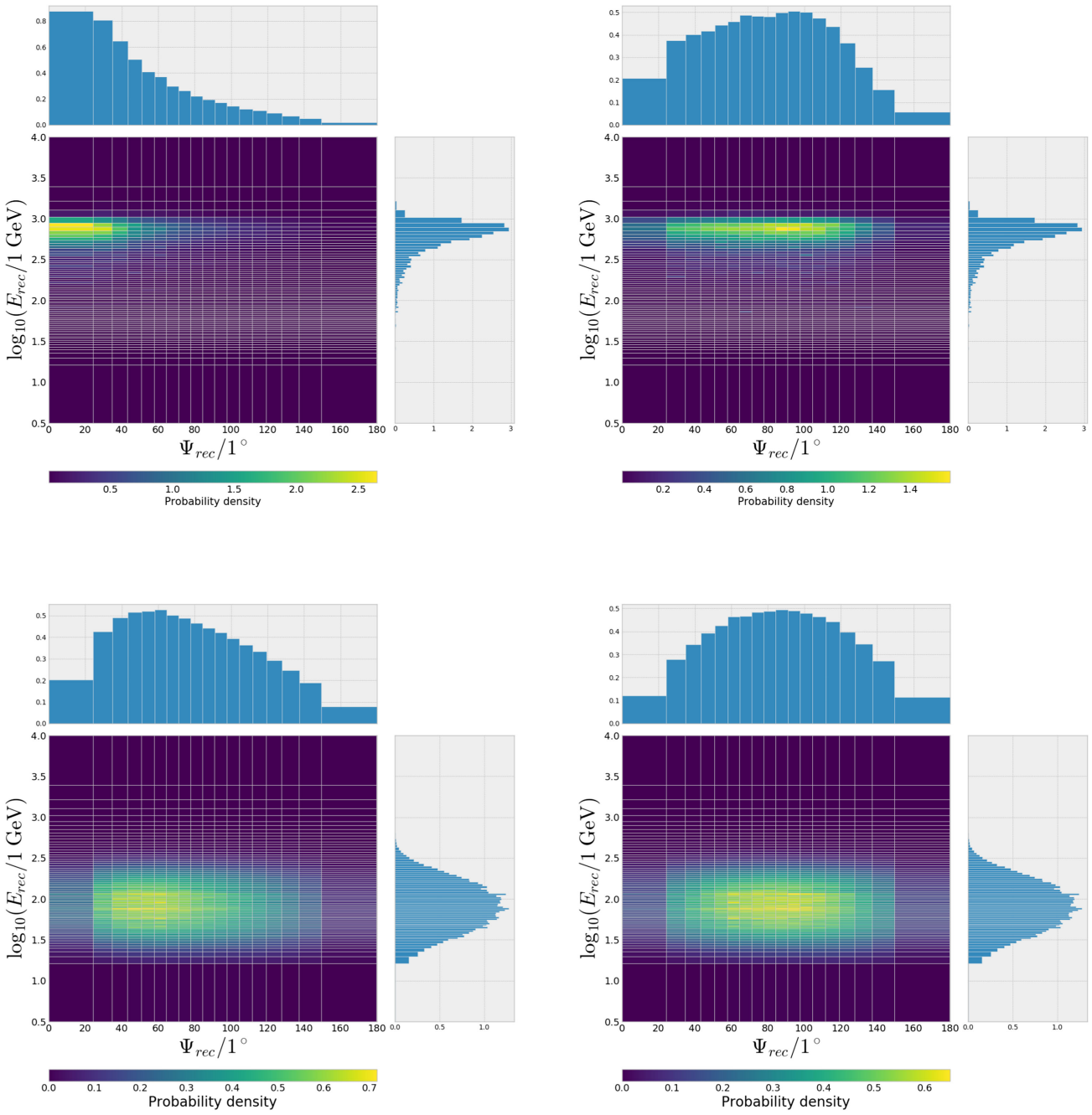

FIG. 3. Top row: signal probability density function for a dark matter particle of $m_\chi = 1$ TeV annihilating to the $\nu_e\bar{\nu}_e$ channel and the NFW profile for the high-energy selection (left) and the same signal distribution but scrambled in right ascension (right). Bottom row: Same distributions for a dark matter decaying into the $b\bar{b}$ channel and assuming the Burkert profile.

Detector systematic uncertainties will, in addition, affect the efficiency of the detector and might introduce a bias in the fitted signal fraction, which will influence the conversion from an estimated number of signal events or upper limits to the physical parameters, $\langle\sigma v\rangle$ and τ_χ. Among the known detector systematic uncertainties we evaluated the DOM efficiency and several ice properties. Variations in the detector parameters, within their systematic uncertainties, result in a 30% uncertainty in the nominal detector sensitivity, below the statistical uncertainties due to fluctuations of the background. These effects on the result are, however, far smaller than the effect due to astrophysical uncertainties. As usual for dark matter indirect searches the latter constitute the dominant source of uncertainty.

In particular, the shape of the dark matter halo profile can have a large impact on the results. For this reason we will consider two typical bracketing halo profiles.

VI. RESULTS FOR THE NEUTRINO-LINE CHANNEL

After performing the likelihood maximization on all the masses and neutrino channels for both halo profiles and for both the annihilation and the decay modes, no significant excess with respect to the background expectation is found. In the absence of such a signal we place upper limits on the thermally averaged annihilation cross section and lower limits on the dark matter decay lifetime. In order to establish upper limits on the signal fraction we used the test statistics defined as [49]

$$q_\mu = \begin{cases} -2\log\frac{\mathcal{L}(\hat{\mu})}{\mathcal{L}(\mu)} & \hat{\mu} \leq \mu, \\ 0 & \hat{\mu} > \mu. \end{cases} \tag{9}$$

An upper limit is built by selecting the value μ producing a significance of 10%, under the same $\mathcal{H}_1(\mu)$ hypothesis. After verifying that the asymptotic distribution of q_μ correctly follows a half χ^2 distribution for 1 degree of freedom as dictated by a generalization [50] of Wilks's theorem [51], we used the value of $q_\mu = 1.64$ to calculate the limits.

Figure 4 shows the upper limits obtained on the thermally averaged annihilation cross section for the $\nu_e\bar{\nu}_e$ final state assuming a NFW (top panel) or Burkert (bottom panel) dark matter halo profile as a function of the dark matter mass. The dotted line indicates the expected median upper limit, or sensitivity, in the absence of signal at one-sided 90% C.L. while the green and yellow bands indicate the 68% and 95% expected background fluctuations. Upper limits are only evaluated at the corresponding mass points and lines in between are only used to guide the eye. Masses below 1 TeV are evaluated with the low-energy dataset while larger masses are tested with the high-energy selection. There is a mild positive fluctuation toward ∼1 TeV in dark matter masses for this neutrino channel. The local significance of this fluctuation does not exceed $\sim 1.3\sigma$ (p-value of ∼10%) and it is visible in both profiles. Due to the quantile binning procedure, at higher energies there is a strong correlation among masses between 10 and 200 TeV which explains why upper limits are consistently above the median sensitivity over such a broad range of masses.

Similar results are obtained for the practically identical signals from the two other neutrino flavors, as shown in Tables I–III in the Appendix.

Results on dark matter decays for the same $\nu_e\bar{\nu}_e$ neutrino channel are summarized in Fig. 5. Because it is the same dataset that is analyzed, limits are again less stringent than the expected sensitivity at energies around 1 TeV and the local signal significance reaches modest values around 2.3σ (p-value of ∼1%).

Figure 6 shows the results of dark matter annihilating (left) and decaying (right) to neutrinos in comparison with other neutrino experiments. These monochromatic neutrino

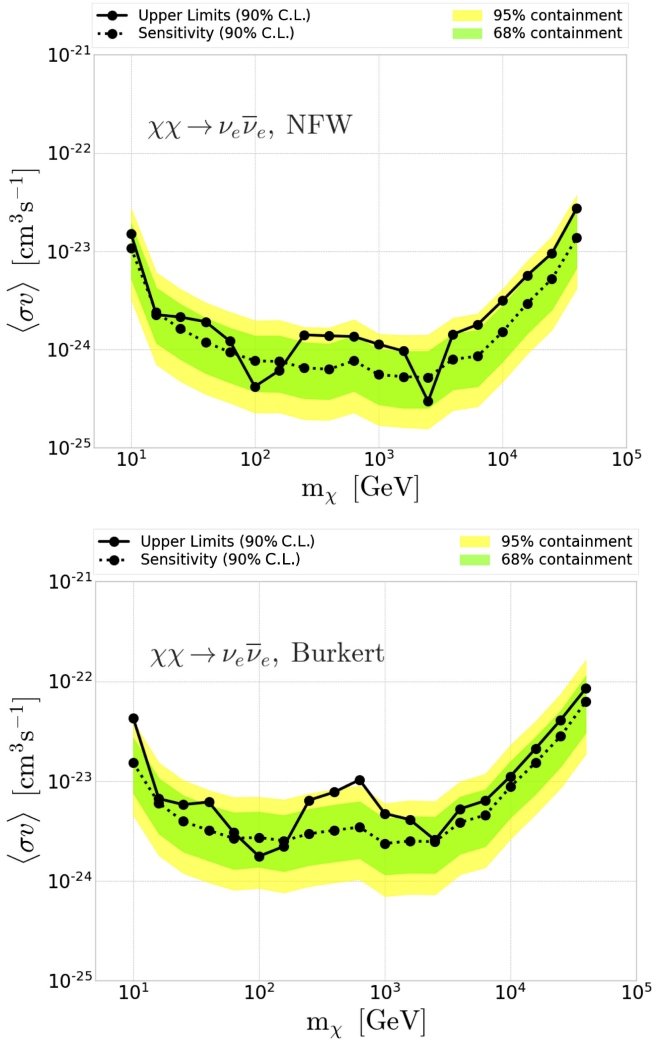

FIG. 4. Upper limits (solid line) and sensitivity (dotted line) at 90% C.L. on the thermally averaged self-annihilation cross section of the $\nu_e\bar{\nu}_e$ channel and NFW profile (top) and Burkert profile (bottom) as function of the dark matter mass together with the 1σ (green) and 2σ (yellow) containment bands for the expected sensitivity.

limits are averaged over our three neutrino flavor channels to reduce the influence of statistical uncertainties in the previously discussed signal PDFs.

In the annihilation mode there is a notable improvement of $\sim\mathcal{O}(10)$ for masses above 100 GeV when compared to IceCube's previous results using a similar event selection and one year of IceCube data [7]. This significant improvement is realized by considering both the angular and energy information of the neutrino events together with additional years of data.

There is still room for further improvement of these limits in the near future. First of all, more years of data are available and will improve IceCube's sensitivity to dark matter. In addition, recent technical improvements within the collaboration, such as better cascade energy and

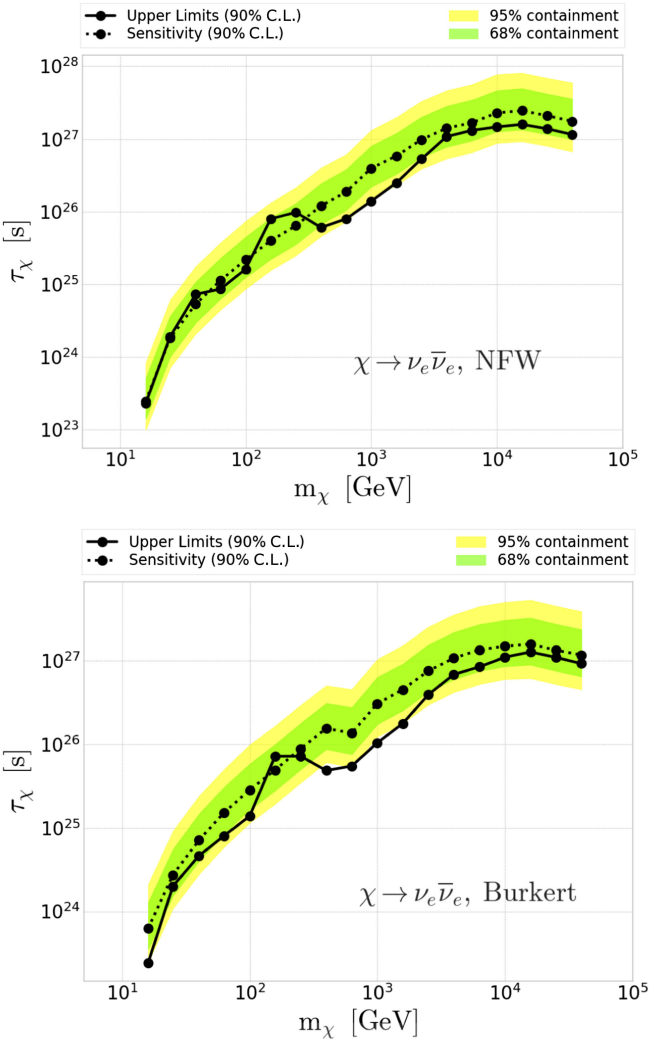

FIG. 5. Lower limits (solid line) and sensitivity (dotted line) at 90% C.L. on the decaying dark matter lifetime τ_χ of the $\nu_e\bar{\nu}_e$ channel for NFW profile (top) and Burkert profile (bottom) as function of the dark matter mass together with the 1σ (green) and 2σ (yellow) containment bands for the expected sensitivity.

directional reconstructions using deep neural networks [56] together with a better understanding and modeling of the ice properties and calibration of the photodetector response functions, will improve the energy resolution making it more sensitive to dark matter monochromatic signatures.

Note also that, even if the $\sim 10^{-24}$ sensitivity reached on $\langle\sigma v\rangle$ in Fig. 4 is a factor $\sim$30 larger than the annihilation cross section at the time of dark matter freeze-out in thermal dark matter frameworks, the Sommerfeld enhancement effect can largely boost this cross section into neutrinos today in the Galactic Center [11]. As a result neutrino telescopes are already testing today thermal scenarios where dark matter annihilates for a large part into neutrinos. This basically only requires that the mediator through which dark matter annihilate into neutrinos is sufficiently lighter than the dark matter particle. This holds for dark matter masses above few TeV if the mediator is an electroweak gauge boson or below if the mediator is a new lighter particle beyond the Standard Model.

VII. RESULTS FOR THE SECONDARY NEUTRINO CHANNELS

For annihilation and decay channels proceeding into a pair of Standard Model charged particles, leading to a continuous energy spectrum of secondary neutrinos, the energy information of the event is less crucial than for a monochromatic line. However, using the energy information of the events still leads to an improvement of the sensitivity.

Using the same data samples as for the neutrino-line searches, no clear deviation from the background hypothesis is observed with any of the dark matter annihilation and decay channels tested. The mild excess of events observed in the $\nu_\alpha\bar{\nu}_\alpha$ channels is also observed for these channels, although at slightly higher masses (this is especially true for the $b\bar{b}$ channel). The most significant excess among all our studied signals shows up for the annihilation into $\tau^+\tau^-$ final states at $\sim$1.5 TeV with the Burkert profile, which yields a pretrial significance of 0.03.

However, correcting for the number of trials—due to the different channels, masses, and dark matter profiles analyzed—by generating background pseudosamples and repeating the analysis, lowers the significance to $\sim$38%, which is well compatible with the background expectations.

In Fig. 7 we show the results for the annihilation into the $\tau^+\tau^-$ channel and the Burkert profile, as well as the results for dark matter decay into W^+W^- with the NFW profile.

The results of all the channels and profiles tested can be found in the Appendix (see Tables IV–VII), together with the plots summarizing all the results.

Figure 8 shows the results obtained for the $\tau^+\tau^-$ channel in comparison with other neutrino and gamma-ray experiments. For the charged particle channels the portion of energy that goes into γ's or $e^\pm$, quickly producing γ rays, is in general large [44]. Thus, combined with the fact that neutrinos have lower detection cross sections, gamma-ray detectors are in general more sensitive to these channels than neutrino telescopes.

It is also interesting to compare the limits obtained above on neutrino pair production by neutrino telescopes with the limits obtained by gamma-ray telescopes on charged lepton pair production. This comparison is interesting because in many models the associated annihilation cross sections are predicted to be basically equal due to $SU(2)_L$ gauge invariance, even if it is known that there also exist other models where the charged pair production is way more suppressed than the neutrino pair production, see [11].

As can be seen in Fig. 8, gamma-ray telescopes are still more sensitive on the dark matter production of $\tau^+\tau^-$ than

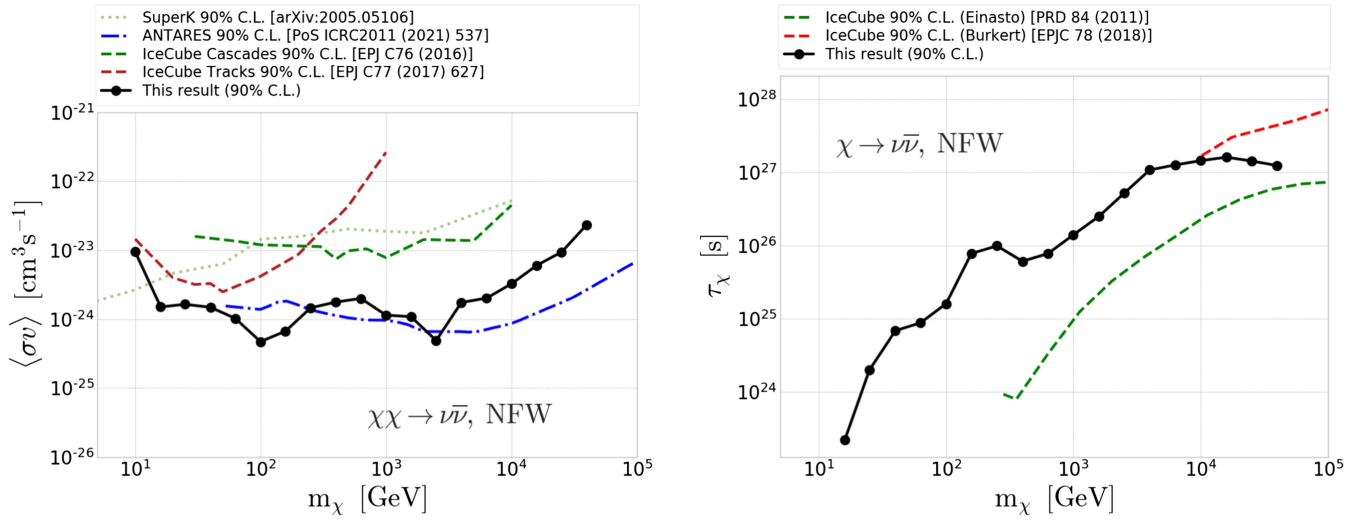

FIG. 6. Left: limits on the thermally averaged cross section for the average $\nu\bar{\nu}$ channels compared to previous IceCube results [7,31] as well as Super-Kamiokande [52] and ANTARES [53]. Right: limits on the decaying lifetime for the average $\nu\bar{\nu}$ channels compared also to previous IceCube limits [54,55].

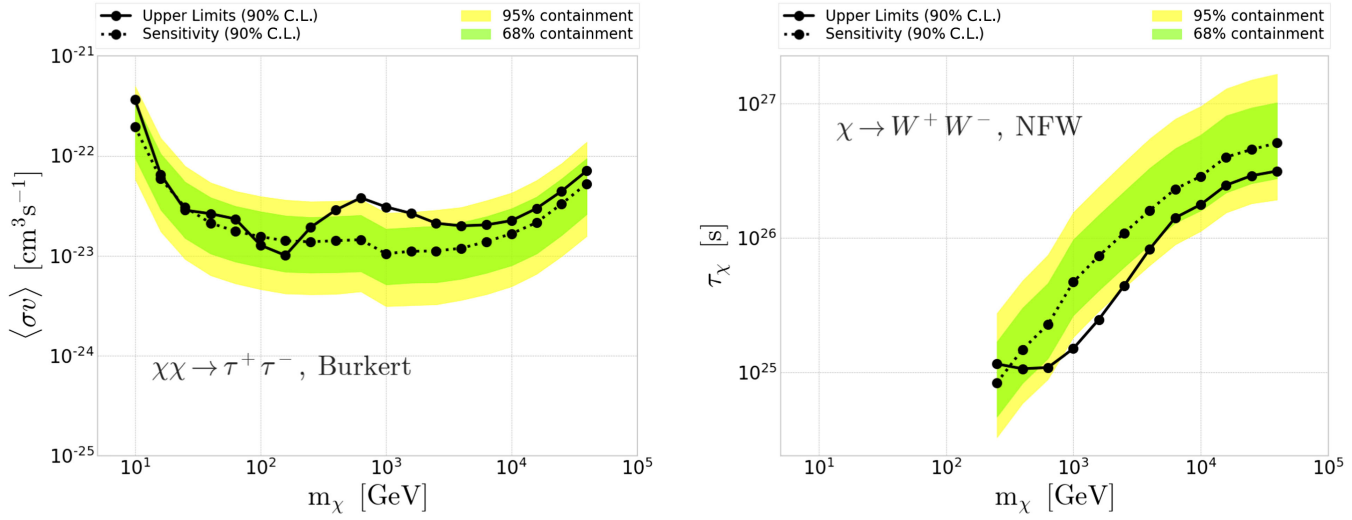

FIG. 7. Left: same as Fig. 4, but for $\tau^+\tau^-$ annihilation channel and Burkert profile. Right: lower limits and sensitivity on the decaying lifetime for W^+W^- and NFW profile.

neutrino telescopes on the production of the $\nu\bar{\nu}$ channel (see Fig. 6) by 1 order of magnitude at masses below few tens of TeV. On the other hand, neutrino telescope limits on the neutrino channel are comparable to gamma-ray limits on the $\mu^+\mu^-$ and e^+e^- channels for masses above a few TeV [60–62].

VIII. CONCLUSION

In this work we showed the results of the first neutrino telescope dedicated search for neutrino lines, using both the spatial and energy information of the neutrino events. The event selections, both the low-energy and the high-energy, are based on a five-year cascade event IceCube/DeepCore data sample [7]. No evidence of dark matter signature was found and new upper limits (lower limits) were set on the annihilation cross section (decay lifetime). The results constitute a large improvement with respect to previous analyses of the order of 1 order of magnitude, except for dark matter masses around 1 TeV where the improvement is less significant due to a mild excess of neutrino events causing weaker dark matter constraints as compared to the expected sensitivity. The same analyses provide competitive limits for dark matter annihilation and decay into charged particles. More available data as well as new advancements in cascade reconstructions and MC will be able to improve these limits in the near future.

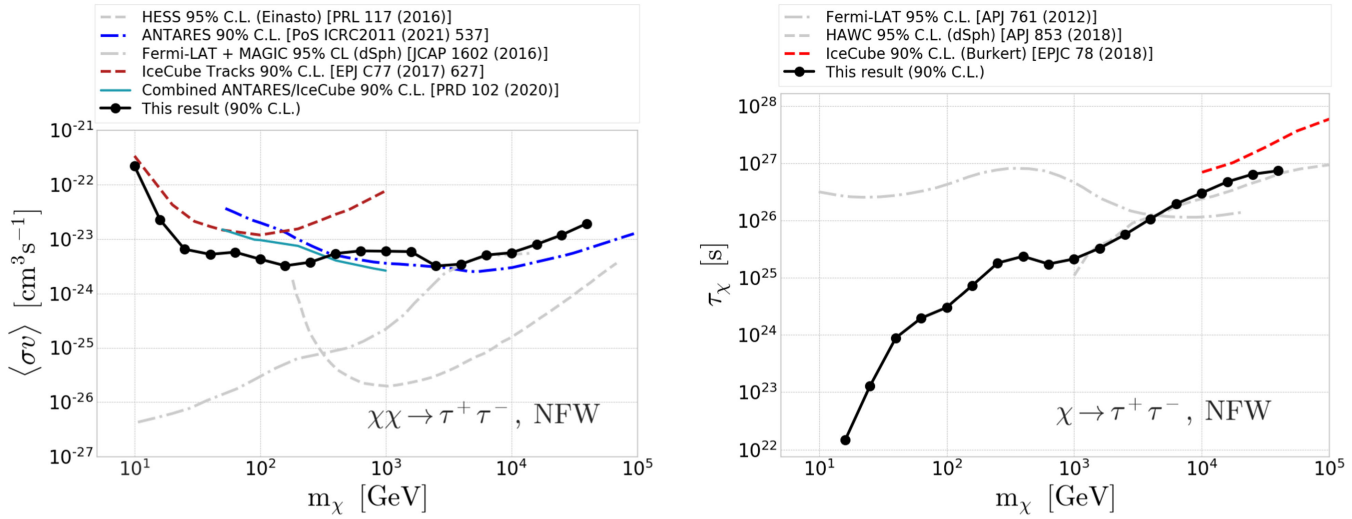

FIG. 8. Left: upper limits on the thermally averaged cross section for the $\tau^+\tau^-$ channel compared to other neutrino detectors, such as previous IceCube results [7,31] and ANTARES [53], and the gamma-ray telescope H.E.S.S [57] and Fermi [58]. Right: lower limits on the dark matter decay lifetime for the $\tau^+\tau^-$ channel compared also to previous IceCube limits [54,55] and HAWC [59].

ACKNOWLEDGMENTS

The IceCube Collaboration acknowledges the significant contributions to this manuscript from J. A. Aguilar, M. Gustafsson, and T. Hambye, as well as support from the following: USA—U.S. National Science Foundation-Office of Polar Programs, U.S. National Science Foundation-Physics Division, Wisconsin Alumni Research Foundation, Center for High Throughput Computing (CHTC) at the University of Wisconsin-Madison, Open Science Grid (OSG), Extreme Science and Engineering Discovery Environment (XSEDE), U.S. Department of Energy-National Energy Research Scientific Computing Center, Particle Astrophysics Research Computing Center at the University of Maryland, Institute for Cyber-Enabled Research at Michigan State University, and Astroparticle Physics Computational Facility at Marquette University; Belgium—Funds for Scientific Research (FRS-FNRS and FWO), FWO Odysseus and Big Science programmes, and Belgian Federal Science Policy Office (Belspo); Germany—Bundesministerium für Bildung und Forschung (BMBF), Deutsche Forschungsgemeinschaft (DFG), Helmholtz Alliance for Astroparticle Physics (HAP), Initiative and Networking Fund of the Helmholtz Association, Deutsches Elektronen Synchrotron (DESY), and High Performance Computing cluster of the RWTH Aachen; Sweden—Swedish Research Council, Swedish Polar Research Secretariat, Swedish National Infrastructure for Computing (SNIC), and Knut and Alice Wallenberg Foundation; Australia—Australian Research Council; Canada—Natural Sciences and Engineering Research Council of Canada, Calcul Québec, Compute Ontario, Canada Foundation for Innovation, WestGrid, and Compute Canada; Denmark—Villum Fonden, Danish National Research Foundation (DNRF); New Zealand—Marsden Fund; Japan—Japan Society for Promotion of Science (JSPS) and Institute for Global Prominent Research (IGPR) of Chiba University; Korea—National Research Foundation of Korea (NRF); Switzerland—Swiss National Science Foundation (SNSF). This particular project has been further supported in Belgium by the Action de recherche concertées (ARC), "Probing dark matter with neutrinos" from the Université Libre de Bruxelles.

APPENDIX: DARK MATTER CONSTRAINTS FROM ALL TESTED ANNIHILATION AND DECAY CHANNELS

Figure 9 shows the limits obtained for an annihilation and decay case for all the annihilation and decay channels tested: $\nu\bar{\nu}$, $\mu^+\mu^-$, $\tau^+\tau^-$, $b\bar{b}$, and W^+W^- channels. The neutrino-line channel is the average from all the three neutrino flavors. These plots summarize the information that can be found in the Tables I–VII.

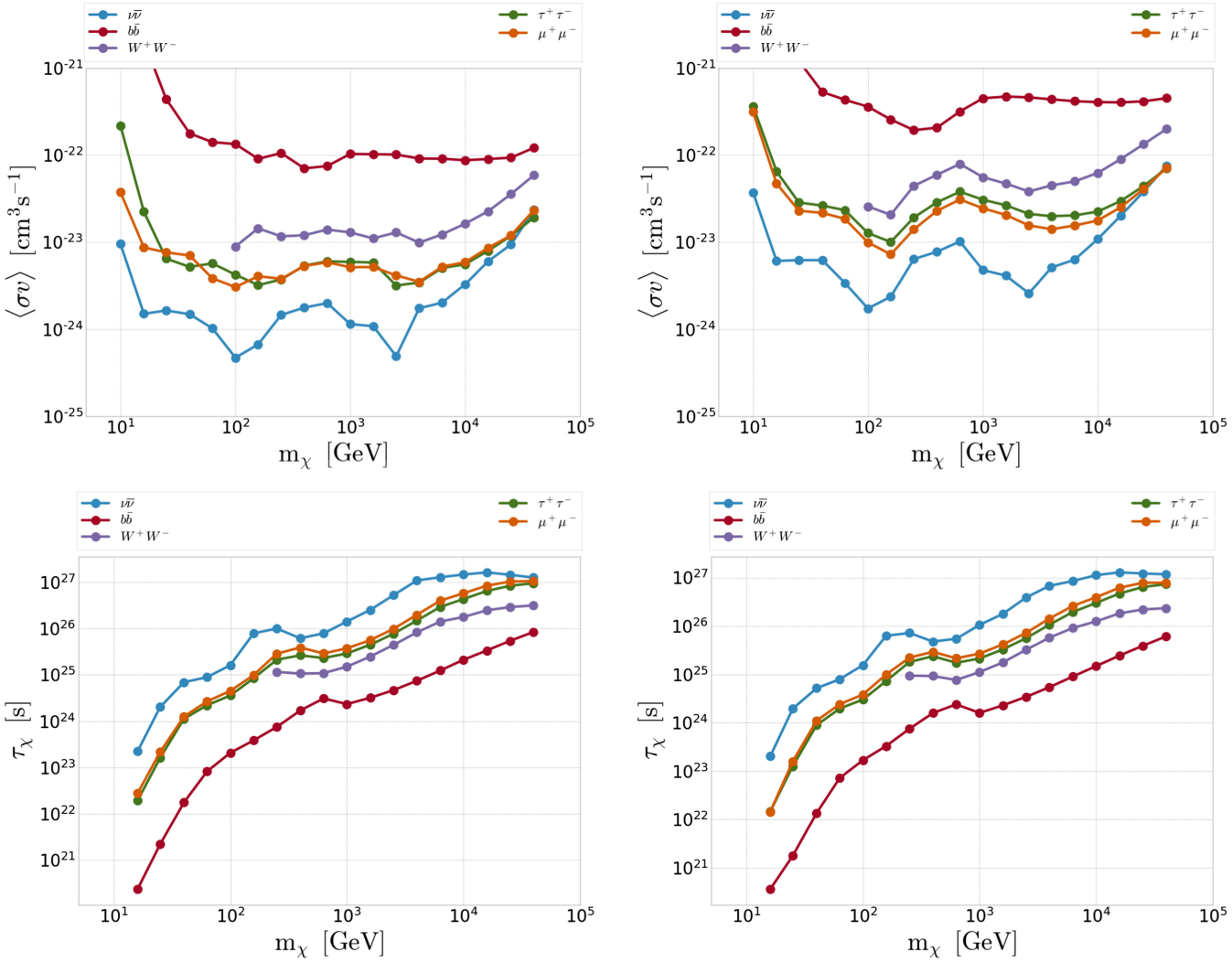

FIG. 9. Top: upper limits for all channels in thermally averaged cross section as function of the dark matter mass for the NFW profile (left) and Burkert profile (right). Bottom: lower limits for all channels in dark matter lifetime as function of the dark matter mass for the NFW profile (left) and Burkert profile (right).

TABLE I. Table with the results for the final state channel $\nu_e\bar{\nu}_e$ for both the annihilation and decaying mode and for both the NFW and Burkert profile. The best fit value on the number of signal evens $\hat{n}_s$ is shown together with the resulting upper limit in $\langle\sigma v\rangle^{90\%}_{\text{u.l.}}$ and lower limit on $\tau^{90\%}_{\text{l.l.}}$ along with the significance given in number of sigmas, z-score.

	Annihilation						Decay					
	NFW			Burkert			NFW			Burkert		
m_χ (GeV)	$\hat{n}_s$	$\langle\sigma v\rangle^{90\%}_{\text{u.l.}}$ 10^{-24} (cm^2)	z-score	$\hat{n}_s$	$\langle\sigma v\rangle^{90\%}_{\text{u.l.}}$ 10^{-24} (cm^2)	z-score	$\hat{n}_s$	$\tau^{90\%}_{\text{l.l.}}$ 10^{24} (s)	z-score	$\hat{n}_s$	$\tau^{90\%}_{\text{l.l.}}$ 10^{24} (s)	z-score
10	51.99	15.01	0.50	8.90	43.02	0.04	...	...	...	...	...	...
16	0.00	2.26	0.00	0.00	6.65	0.00	24.36	0.23	0.10	0.01	0.24	0.00
25	68.06	2.14	0.41	2.44	5.81	0.01	0.00	1.90	0.00	0.00	2.00	0.00
40	132.26	1.92	0.79	142.46	6.16	0.45	0.00	7.26	0.00	0.21	4.63	0.00
63	48.95	1.21	0.36	0.00	3.06	0.00	203.34	8.57	0.41	53.77	8.04	0.09
100	0.00	0.42	0.00	0.00	1.76	0.00	207.92	16.20	0.45	131.84	13.80	0.22
158	0.00	0.61	0.00	0.00	2.21	0.00	0.00	79.06	0.00	0.00	71.83	0.00
251	68.15	1.41	1.41	162.78	6.43	1.58	0.00	97.71	0.00	0.00	71.84	0.00
398	44.22	1.38	1.32	137.11	7.75	1.79	215.76	60.16	1.22	209.89	48.45	0.87
631	20.81	1.35	0.77	123.15	10.30	1.94	232.55	79.23	1.69	320.05	54.84	1.73
1000	58.75	1.13	1.27	116.62	4.73	1.22	397.88	139.26	2.29	491.00	103.89	2.15
1585	32.94	0.96	0.95	67.87	4.11	0.95	277.51	248.91	1.70	369.96	177.36	1.73
2512	0.00	0.30	0.00	0.00	2.57	0.00	135.46	528.81	1.11	165.28	391.76	1.02
3981	21.03	1.43	1.11	27.53	5.26	0.61	32.34	1079.73	0.31	72.36	683.29	0.54
6310	21.03	1.79	1.43	21.62	6.36	0.64	29.86	1310.17	0.36	54.86	841.87	0.48
10000	18.93	3.13	1.40	19.86	11.16	0.63	45.25	1463.26	0.83	46.25	1097.92	0.60
15850	16.38	5.67	1.25	18.84	21.18	0.62	38.10	1584.29	0.78	31.83	1266.47	0.46
25120	13.64	9.54	1.21	17.56	41.11	0.61	33.71	1379.79	0.74	26.28	1092.62	0.40
39810	17.94	27.30	1.33	18.46	84.87	0.64	33.64	1150.55	0.79	26.17	922.08	0.43

TABLE II. Same as table I for the $\nu_\mu\bar{\nu}_\mu$ channel. Since we assumed a democratic neutrino flavor compositions of the signals at the detector, any differences among the tables are dominantly due to statistical fluctuations between the signals' generated PDFs.

	Annihilation						Decay					
	NFW			Burkert			NFW			Burkert		
m_χ (GeV)	$\hat{n}_s$	$\langle\sigma v\rangle^{90\%}_{\text{u.l.}}$ 10^{-24} (cm^2)	z-score	$\hat{n}_s$	$\langle\sigma v\rangle^{90\%}_{\text{u.l.}}$ 10^{-24} (cm^2)	z-score	$\hat{n}_s$	$\tau^{90\%}_{\text{u.l.}}$ 10^{24} (s)	z-score	$\hat{n}_s$	$\tau^{90\%}_{\text{u.l.}}$ 10^{24} (s)	z-score
10	27.65	8.60	0.47	0.00	37.50	0.00	...	...	...	...	...	...
16	0.00	1.27	0.00	0.00	5.61	0.00	30.20	0.22	0.12	78.38	0.16	0.27
25	0.00	1.24	0.00	39.96	6.37	0.13	0.00	2.19	0.00	0.73	1.46	0.00
40	0.00	1.14	0.00	131.83	6.00	0.42	0.00	6.78	0.00	0.00	5.53	0.00
63	0.01	1.04	0.00	0.00	3.57	0.00	152.05	9.11	0.31	37.92	8.13	0.06
100	0.00	0.44	0.00	0.00	1.74	0.00	218.75	15.92	0.47	0.00	17.62	0.00
158	0.00	0.58	0.00	0.00	2.57	0.00	0.00	73.24	0.00	0.00	59.21	0.00
251	70.75	1.40	1.27	159.23	6.34	1.55	0.00	99.24	0.00	0.00	78.70	0.00
398	68.09	2.09	1.69	141.16	7.87	1.84	194.77	62.38	1.07	205.03	48.75	0.84
631	36.75	2.20	1.09	120.84	10.15	1.89	241.20	77.63	1.74	323.28	54.62	1.75
1000	65.46	1.24	1.24	118.37	4.75	1.23	397.15	139.88	2.30	468.35	107.05	2.05
1585	23.72	1.07	0.59	69.60	4.13	0.97	270.54	253.60	1.66	370.16	177.54	1.72
2512	0.01	0.58	0.00	0.02	2.58	0.00	142.02	518.33	1.15	171.01	387.55	1.05
3981	24.79	1.85	1.13	25.04	5.02	0.55	35.16	1089.38	0.34	77.10	681.11	0.57
6310	18.17	2.01	1.14	22.41	6.25	0.64	38.00	1237.17	0.44	56.26	843.13	0.48
10000	24.25	3.69	1.60	20.93	10.66	0.65	49.90	1423.89	0.87	45.37	1128.16	0.57
15850	22.15	6.45	1.48	19.59	19.46	0.63	38.22	1654.79	0.76	33.78	1304.98	0.48
25120	14.89	9.57	1.28	18.57	36.17	0.62	34.14	1494.90	0.73	28.97	1151.67	0.43
39810	17.03	20.15	1.46	18.17	70.14	0.62	32.56	1314.54	0.74	0.00	1576.34	0.00

TABLE III. Same as table I for the $\nu_\tau\bar{\nu}_\tau$ channel. Since we assumed a democratic neutrino flavor compositions of the signals at the detector, any differences among the tables are dominantly due to statistical fluctuations between the signals' generated PDFs.

	Annihilation						Decay					
	NFW			Burkert			NFW			Burkert		
m_χ (GeV)	$\hat{n}_s$	$\langle\sigma v\rangle^{90\%}_{\text{u.l.}}$ 10^{-24} (cm^2)	z-score	$\hat{n}_s$	$\langle\sigma v\rangle^{90\%}_{\text{u.l.}}$ 10^{-24} (cm^2)	z-score	$\hat{n}_s$	$\tau^{90\%}_{\text{u.l.}}$ 10^{24} (s)	z-score	$\hat{n}_s$	$\tau^{90\%}_{\text{u.l.}}$ 10^{24} (s)	z-score
10	0.01	5.17	0.00	0.00	31.36	0.00	…	…	…	…	…	…
16	0.00	0.98	0.00	0.00	6.04	0.00	31.15	0.22	0.12	6.49	0.20	0.02
25	17.12	1.55	0.12	48.89	6.49	0.16	0.00	1.96	0.00	0.00	2.42	0.00
40	31.65	1.40	0.20	173.99	6.53	0.55	0.00	6.67	0.00	0.00	5.34	0.00
63	0.00	0.83	0.00	0.00	3.58	0.00	184.14	8.83	0.38	95.94	7.59	0.15
100	0.00	0.56	0.00	0.00	1.69	0.00	206.01	16.19	0.45	66.11	14.91	0.11
158	0.00	0.81	0.00	0.00	2.30	0.00	0.00	83.23	0.00	0.00	57.91	0.00
251	86.37	1.57	1.49	162.47	6.43	1.58	0.00	102.25	0.00	0.14	65.23	0.00
398	55.98	1.84	1.48	136.87	7.70	1.79	202.46	62.01	1.14	235.25	46.44	0.98
631	46.98	2.43	1.44	119.94	10.15	1.87	235.96	78.56	1.71	325.58	54.40	1.76
1000	46.34	1.06	0.87	125.21	4.88	1.30	377.12	144.53	2.18	475.38	106.10	2.08
1585	33.36	1.21	0.84	72.25	4.20	1.01	272.23	252.43	1.67	358.44	181.06	1.67
2512	0.00	0.59	0.00	0.02	2.61	0.00	138.05	525.37	1.12	168.37	390.51	1.03
3981	26.26	1.95	1.15	27.16	5.16	0.59	35.13	1088.77	0.34	79.86	669.90	0.59
6310	22.50	2.26	1.38	22.59	6.31	0.64	36.43	1265.33	0.43	50.88	865.59	0.44
10000	18.16	3.00	1.35	21.13	10.74	0.66	47.30	1470.41	0.84	44.03	1148.93	0.56
15850	19.28	5.98	1.29	19.94	19.73	0.63	40.21	1618.85	0.79	33.85	1282.60	0.47
25120	13.84	9.17	1.16	19.80	36.90	0.66	36.48	1442.87	0.77	0.00	1415.95	0.00
39810	21.64	22.87	1.75	19.93	71.50	0.66	34.10	1275.83	0.76	13.62	1018.97	0.18

TABLE IV. Same as table I for the $b\bar{b}$ channel.

	Annihilation						Decay					
	NFW			Burkert			NFW			Burkert		
m_χ (GeV)	$\hat{n}_s$	$\langle\sigma v\rangle^{90\%}_{\text{u.l.}}$ 10^{-24} (cm^2)	z-score	$\hat{n}_s$	$\langle\sigma v\rangle^{90\%}_{\text{u.l.}}$ 10^{-24} (cm^2)	z-score	$\hat{n}_s$	$\tau^{90\%}_{\text{u.l.}}$ 10^{24} (s)	z-score	$\hat{n}_s$	$\tau^{90\%}_{\text{u.l.}}$ 10^{24} (s)	z-score
10	41.34	9340.72	0.53	25.05	22335.36	0.19	…	…	…	…	…	…
16	63.32	2029.91	0.57	0.00	4620.84	0.00	80.40	0.00	0.46	0.00	0.00	0.00
25	4.98	439.28	0.03	0.00	1208.43	0.00	31.76	0.00	0.12	20.79	0.00	0.07
40	0.00	177.03	0.00	0.00	529.93	0.00	0.31	0.02	0.00	0.00	0.01	0.00
63	34.33	140.57	0.18	0.04	432.09	0.00	0.10	0.08	0.00	0.00	0.07	0.00
100	127.42	133.51	0.60	45.81	358.84	0.12	0.00	0.21	0.00	0.00	0.17	0.00
158	67.91	90.43	0.32	0.00	255.22	0.00	0.08	0.38	0.00	0.00	0.33	0.00
251	99.51	105.18	0.47	0.00	192.89	0.00	16.88	0.75	0.03	0.00	0.75	0.00
398	56.28	70.32	0.32	0.00	205.67	0.00	0.00	1.69	0.00	0.00	1.58	0.00
631	109.59	74.69	0.76	196.62	315.35	0.64	0.14	3.08	0.00	0.00	2.40	0.00
1000	207.59	102.94	2.00	444.50	449.47	2.07	366.60	2.33	1.12	525.96	1.60	1.22
1585	233.26	102.09	2.31	516.36	469.91	2.42	623.24	3.19	1.89	821.49	2.28	1.89
2512	229.47	101.20	2.37	498.33	460.13	2.44	802.91	4.65	2.45	1003.51	3.44	2.31
3981	182.86	91.19	2.04	425.56	436.13	2.26	820.11	7.41	2.58	1044.57	5.41	2.49
6310	156.50	90.63	1.94	341.57	415.65	2.02	737.14	12.30	2.47	936.61	8.99	2.38
10000	122.11	87.24	1.78	263.93	405.73	1.79	591.45	20.92	2.19	789.43	14.76	2.19
15850	98.44	89.93	1.73	197.21	402.38	1.58	486.66	33.27	2.01	618.35	24.31	1.93
25120	71.63	93.29	1.50	144.07	414.40	1.36	369.04	53.94	1.79	475.30	38.83	1.72
39810	63.13	121.20	1.60	106.67	450.63	1.18	275.71	84.10	1.58	343.97	61.36	1.46

TABLE V. Same as table I for the W^+W^- channel.

	Annihilation						Decay					
	NFW			Burkert			NFW			Burkert		
m_χ (GeV)	$\hat{n}_s$	$\langle\sigma v\rangle^{90\%}_{\text{u.l.}}$ 10^{-24} (cm^2)	z-score	$\hat{n}_s$	$\langle\sigma v\rangle^{90\%}_{\text{u.l.}}$ 10^{-24} (cm^2)	z-score	$\hat{n}_s$	$\tau^{90\%}_{\text{u.l.}}$ 10^{24} (s)	z-score	$\hat{n}_s$	$\tau^{90\%}_{\text{u.l.}}$ 10^{24} (s)	z-score
100	0.01	8.93	0.00	0.00	25.72	0.00	...	...	...	...	...	...
158	108.67	14.42	0.68	0.00	20.62	0.00	...	...	...	...	...	...
251	103.96	11.68	1.16	162.95	44.30	0.89	0.00	11.50	0.00	0.00	9.42	0.00
398	96.87	12.03	1.45	244.93	59.29	1.69	60.08	10.59	0.18	0.01	9.22	0.00
631	78.34	13.98	1.36	267.65	78.94	2.14	338.60	10.81	1.38	446.23	7.64	1.35
1000	156.43	12.94	2.15	325.55	55.74	2.19	633.39	14.94	2.65	783.64	11.13	2.48
1585	105.55	11.06	1.71	210.19	46.99	1.68	555.29	24.61	2.38	730.95	17.63	2.37
2512	100.09	12.94	1.59	99.67	38.16	0.93	403.61	44.08	1.94	512.46	32.23	1.88
3981	37.32	9.89	0.83	83.27	44.92	0.88	237.28	82.50	1.34	328.46	57.55	1.41
6310	41.74	12.30	1.28	66.79	49.85	0.91	128.47	140.78	0.84	210.19	90.99	1.02
10000	39.78	16.29	1.40	57.08	62.30	0.91	133.24	176.62	1.07	171.72	124.80	0.99
15850	38.02	22.61	1.45	54.08	89.70	0.91	104.07	246.60	1.03	117.88	182.60	0.84
25120	37.98	35.68	1.47	51.32	133.40	0.89	92.33	289.76	1.01	97.55	220.01	0.76
39810	36.53	58.84	1.51	48.12	199.24	0.86	87.95	313.58	1.01	96.77	234.15	0.79

TABLE VI. Same as table I for the $\tau^+\tau^-$ channel.

	Annihilation						Decay					
	NFW			Burkert			NFW			Burkert		
m_χ (GeV)	$\hat{n}_s$	$\langle\sigma v\rangle^{90\%}_{\text{u.l.}}$ 10^{-24} (cm^2)	z-score	$\hat{n}_s$	$\langle\sigma v\rangle^{90\%}_{\text{u.l.}}$ 10^{-24} (cm^2)	z-score	$\hat{n}_s$	$\tau^{90\%}_{\text{u.l.}}$ 10^{24} (s)	z-score	$\hat{n}_s$	$\tau^{90\%}_{\text{u.l.}}$ 10^{24} (s)	z-score
10	97.09	217.83	0.92	0.04	363.10	0.00	...	...	...	...	...	...
16	0.05	22.32	0.00	0.00	64.80	0.00	214.63	0.02	2.19	68.44	0.01	0.25
25	0.00	6.48	0.00	0.00	28.54	0.00	0.00	0.16	0.00	0.00	0.13	0.00
40	0.01	5.21	0.00	29.84	26.28	0.08	0.00	1.12	0.00	0.10	0.89	0.00
63	0.03	5.72	0.00	88.01	23.31	0.24	0.38	2.20	0.00	0.00	1.96	0.00
100	11.57	4.24	0.07	0.00	12.74	0.00	112.26	3.57	0.20	39.05	3.01	0.06
158	0.00	3.22	0.00	0.00	10.06	0.00	1.09	8.36	0.00	0.08	7.25	0.00
251	25.75	3.74	0.26	87.68	19.21	0.40	0.00	21.10	0.00	0.00	18.02	0.00
398	80.11	5.40	1.14	230.48	28.64	1.41	0.00	26.18	0.00	0.00	23.62	0.00
631	69.87	6.03	1.25	267.84	37.93	2.06	281.87	22.88	0.99	315.87	17.34	0.83
1000	162.30	5.95	2.45	384.23	30.72	2.43	631.29	28.75	2.47	787.90	21.27	2.33
1585	129.09	5.85	2.03	272.62	26.52	1.99	647.18	44.33	2.62	814.07	32.66	2.50
2512	29.90	3.19	0.57	144.80	21.09	1.28	512.25	77.18	2.26	649.87	56.54	2.18
3981	23.89	3.44	0.60	82.87	19.87	0.88	319.50	148.42	1.69	415.80	106.52	1.66
6310	39.10	5.06	1.28	56.45	20.33	0.81	151.08	290.62	0.96	230.33	194.68	1.11
10000	25.43	5.58	1.17	38.35	22.42	0.73	111.20	430.45	0.89	151.98	300.26	0.91
15850	23.29	7.95	1.25	30.63	29.69	0.70	79.20	643.16	0.88	91.74	469.49	0.73
25120	22.11	11.85	1.38	25.83	44.15	0.66	60.25	832.27	0.85	59.54	638.93	0.60
39810	19.49	19.24	1.28	22.70	70.53	0.66	48.56	945.58	0.80	44.47	733.32	0.52

TABLE VII. Same as table I for the $\mu^+\mu^-$ channel.

	Annihilation						Decay					
	NFW			Burkert			NFW			Burkert		
m_χ (GeV)	$\hat{n}_s$	$\langle\sigma v\rangle^{90\%}_{\text{u.l.}}$ 10^{-24} (cm^2)	z-score	$\hat{n}_s$	$\langle\sigma v\rangle^{90\%}_{\text{u.l.}}$ 10^{-24} (cm^2)	z-score	$\hat{n}_s$	$\tau^{90\%}_{\text{u.l.}}$ 10^{24} (s)	z-score	$\hat{n}_s$	$\tau^{90\%}_{\text{u.l.}}$ 10^{24} (s)	z-score
10	0.01	37.44	0.00	22.31	311.43	0.13	…	…	…	…	…	…
16	0.01	8.71	0.00	0.20	47.20	0.00	186.02	0.03	2.00	184.94	0.01	0.66
25	50.04	7.65	0.43	0.18	22.97	0.00	0.00	0.22	0.00	0.00	0.16	0.00
40	121.75	7.04	0.80	53.54	21.68	0.15	0.16	1.26	0.00	0.00	1.10	0.00
63	15.90	3.86	0.10	91.12	18.53	0.25	0.01	2.66	0.00	0.00	2.41	0.00
100	0.00	3.06	0.00	0.00	9.95	0.00	127.16	4.50	0.23	36.28	3.82	0.05
158	17.97	4.08	0.12	0.00	7.25	0.00	14.22	9.80	0.03	0.00	9.91	0.00
251	34.25	3.80	0.37	49.61	14.04	0.25	0.00	28.47	0.00	0.00	22.16	0.00
398	84.91	5.33	1.26	203.61	22.85	1.42	0.00	38.65	0.00	0.00	29.17	0.00
631	73.61	5.88	1.47	236.07	30.91	2.10	252.54	28.76	1.00	293.35	21.39	0.86
1000	142.61	5.17	2.06	356.56	24.50	2.42	579.06	37.10	2.41	750.01	26.76	2.35
1585	116.00	5.18	1.82	236.63	20.55	1.88	598.32	56.02	2.60	747.97	41.54	2.46
2512	51.84	4.16	0.95	109.62	15.56	1.08	457.70	98.58	2.19	572.94	72.77	2.08
3981	27.95	3.52	0.77	50.88	14.11	0.61	259.20	197.61	1.53	333.22	142.71	1.48
6310	38.13	5.25	1.44	39.28	15.53	0.66	107.25	396.86	0.78	172.73	260.16	0.94
10000	27.37	5.90	1.45	28.31	17.74	0.64	77.02	573.12	0.71	106.84	393.47	0.72
15850	23.98	8.59	1.44	23.38	25.14	0.64	56.53	835.23	0.75	62.00	618.02	0.59
25120	17.36	11.99	1.21	20.73	40.82	0.63	45.37	1027.81	0.77	42.72	784.36	0.52
39810	18.33	23.40	1.28	19.11	71.71	0.62	39.57	1055.78	0.77	33.58	787.77	0.43

[1] J. M. Gaskins, Contemp. Phys. **57**, 496 (2016).
[2] C. Pérez de los Heros, Symmetry **12**, 1648 (2020).
[3] C. A. Argüelles, A. Diaz, A. Kheirandish, A. Olivares-Del-Campo, I. Safa, and A. C. Vincent, Rev. Mod. Phys. **93**, 035007 (2021).
[4] M. Aartsen *et al.* (IceCube Collaboration), Eur. Phys. J. C **77**, 146 (2017); **79**, 214(E) (2019).
[5] S. Adrian-Martinez *et al.* (ANTARES Collaboration), Phys. Lett. B **759**, 69 (2016).
[6] M. Aartsen *et al.* (IceCube Collaboration), Eur. Phys. J. C **77**, 82 (2017).
[7] M. Aartsen *et al.* (IceCube Collaboration), Eur. Phys. J. C **76**, 531 (2016).
[8] M. G. Aartsen *et al.* (IceCube Collaboration), J. Instrum. **9**, P03009 (2014).
[9] C. Garcia-Cely and A. Rivera, J. Cosmol. Astropart. Phys. 03 (2017) 054.
[10] M. Lindner, A. Merle, and V. Niro, Phys. Rev. D **82**, 123529 (2010).
[11] C. El Aisati, C. Garcia-Cely, T. Hambye, and L. Vanderheyden, J. Cosmol. Astropart. Phys. 10 (2017) 021.
[12] F. Takayama and M. Yamaguchi, Phys. Lett. B **485**, 388 (2000).
[13] L. Covi, M. Grefe, A. Ibarra, and D. Tran, J. Cosmol. Astropart. Phys. 01 (2009) 029.
[14] J. Hisano, M. Kawasaki, K. Kohri, and K. Nakayama, Phys. Rev. D **79**, 043516 (2009).
[15] W.-L. Guo, Y.-L. Wu, and Y.-F. Zhou, Phys. Rev. D **81**, 075014 (2010).
[16] M. Garny, A. Ibarra, D. Tran, and C. Weniger, J. Cosmol. Astropart. Phys. 01 (2011) 032.
[17] B. Feldstein, A. Kusenko, S. Matsumoto, and T. T. Yanagida, Phys. Rev. D **88**, 015004 (2013).
[18] T. Higaki, R. Kitano, and R. Sato, J. High Energy Phys. 07 (2014) 044.
[19] C. Rott, K. Kohri, and S. C. Park, Phys. Rev. D **92**, 023529 (2015).
[20] A. Esmaili, S. K. Kang, and P. D. Serpico, J. Cosmol. Astropart. Phys. 12 (2014) 054.
[21] E. Dudas, Y. Mambrini, and K. A. Olive, Phys. Rev. D **91**, 075001 (2015).
[22] C. El Aisati, M. Gustafsson, T. Hambye, and T. Scarna, Phys. Rev. D **93**, 043535 (2016).
[23] C. Garcia-Cely and J. Heeck, J. High Energy Phys. 05 (2017) 102.
[24] H. H. Patel, S. Profumo, and B. Shakya, Phys. Rev. D **101**, 095001 (2020).
[25] R. Coy and T. Hambye, J. High Energy Phys. 05 (2021) 101.
[26] R. Coy, A. Gupta, and T. Hambye, Phys. Rev. D **104**, 083024 (2021).

[27] C. A. Argüelles, D. Delgado, A. Friedlander, A. Kheirandish, I. Safa, A. C. Vincent, and H. White, arXiv:2210.01303.
[28] R. Abbasi *et al.* (IceCube Collaboration), Phys. Rev. D **84**, 022004 (2011).
[29] R. Abbasi *et al.* (IceCube Collaboration), arXiv:1210.3557.
[30] M. G. Aartsen *et al.* (IceCube Collaboration), Eur. Phys. J. C **75**, 492 (2015).
[31] M. Aartsen *et al.* (IceCube Collaboration), Eur. Phys. J. C **77**, 627 (2017).
[32] C. E. Aisati, M. Gustafsson, and T. Hambye, Phys. Rev. D **92**, 123515 (2015).
[33] J. F. Beacom, N. F. Bell, and G. D. Mack, Phys. Rev. Lett. **99**, 231301 (2007).
[34] H. Yuksel, S. Horiuchi, J. F. Beacom, and S. Ando, Phys. Rev. D **76**, 123506 (2007).
[35] M. Aartsen *et al.* (IceCube Collaboration), J. Instrum. **12**, P03012 (2017).
[36] R. Abbasi *et al.* (IceCube Collaboration), Nucl. Instrum. Methods Phys. Res., Sect. A **618**, 139 (2010).
[37] R. Abbasi *et al.* (IceCube Collaboration), Astropart. Phys. **35**, 615 (2012).
[38] A. Hoecker *et al.*, arXiv:physics/0703039.
[39] F. S. Queiroz, W. Rodejohann, and C. E. Yaguna, Phys. Rev. D **95**, 095010 (2017).
[40] J. F. Navarro, C. S. Frenk, and S. D. White, Astrophys. J. **462**, 563 (1996).
[41] A. Burkert, IAU Symp. **171**, 175 (1996).
[42] M. Benito, A. Cuoco, and F. Iocco, J. Cosmol. Astropart. Phys. 03 (2019) 033.
[43] F. Nesti and P. Salucci, J. Cosmol. Astropart. Phys. 07 (2013) 016.
[44] M. Cirelli, G. Corcella, A. Hektor, G. Hutsi, M. Kadastik, P. Panci, M. Raidal, F. Sala, and A. Strumia, J. Cosmol. Astropart. Phys. 03 (2011) 051; 10 (2012) E01.
[45] P. Ciafaloni *et al.*, J. Cosmol. Astropart. Phys. 03 (2011) 019.
[46] C. W. Bauer, N. L. Rodd, and B. R. Webber, J. High Energy Phys. 06 (2021) 121.
[47] C. Giunti and C. W. Kim, *Fundamentals of Neutrino Physics and Astrophysics* (Oxford University Press, 2007).
[48] Ángeles Moliné, A. Ibarra, and S. Palomares-Ruiz, J. Cosmol. Astropart. Phys. 06 (2015) 005.
[49] G. Cowan, K. Cranmer, E. Gross, and O. Vitells, Eur. Phys. J. C Part. Fields **71**, 1 (2011).
[50] H. Chernoff, Ann. Math. Stat. **25**, 573 (1954).
[51] S. S. Wilks, Ann. Math. Stat. **9**, 60 (1938).
[52] K. Abe *et al.*, Phys. Rev. D **102**, 072002 (2020).
[53] M. Ageron *et al.* (ANTARES Collaboration), Proc. Sci. ICRC2021 (**2021**) 537.
[54] R. Abbasi *et al.* (IceCube Collaboration), Phys. Rev. D **84**, 022004 (2011).
[55] M. G. Aartsen *et al.* (IceCube Collaboration), Eur. Phys. J. C **78**, 831 (2018).
[56] R. Abbasi *et al.* (IceCube Collaboration), J. Instrum. **16**, P07041 (2021).
[57] H. Abdallah *et al.* (H.E.S.S. Collaboration), Phys. Rev. Lett. **117**, 111301 (2016).
[58] M. Ahnen *et al.* (MAGIC, Fermi-LAT Collaborations), J. Cosmol. Astropart. Phys. 02 (2016) 039.
[59] A. Albert *et al.* (HAWC Collaboration), Astrophys. J. **853** (2018) 154.
[60] M. L. Ahnen *et al.* (MAGIC, Fermi-LAT Collaborations), J. Cosmol. Astropart. Phys. 02 (2016) 039.
[61] I. John and T. Linden, J. Cosmol. Astropart. Phys. 12 (2021) 007.
[62] L. Bergstrom, T. Bringmann, I. Cholis, D. Hooper, and C. Weniger, Phys. Rev. Lett. **111**, 171101 (2013).